

WIND TUNNEL TESTING OF A HELICOPTER FUSELAGE AND ROTOR IN A SHIP AIRWAKE

Richard G. Lee* and Steven J. Zan†
Aerodynamics Laboratory, Institute for Aerospace Research
National Research Council Canada
Ottawa, Canada

Abstract

The demanding task of landing a maritime helicopter on a ship at sea is constrained by an operational envelope that places limits on wind direction and speed. An operational envelope is normally developed by first-of-class flight trials, but flight testing is an expensive means of qualifying a helicopter for shipborne operations. This paper describes the development of an experimentally-based simulation method which is intended to complement flight testing and mitigate its cost. The basis of the methodology lies with establishing correlations of unsteady aerodynamic fuselage loads (measured in a wind tunnel) with pilot workload (obtained by flight test), assessed for cases where airwake turbulence is chiefly responsible for the workload. With these correlations, contours of unsteady fuselage loading can assist with the definition of the operational envelope.

An experiment was conducted to measure the unsteady aerodynamic fuselage loads in a wind tunnel. In this investigation the fuselage of a Sea King helicopter was immersed in both the downwash of a spinning main rotor and the airwake of a Canadian Patrol Frigate. Measurements of unsteady side force, yawing moment and drag force were made over a combination of wind directions, speeds, and hover positions. The results indicate that a spinning main rotor generating appropriate levels of thrust is a necessary feature of the wind-tunnel simulation. Specifically, in comparison to the rotorless case unsteady loading at low hover over the flight deck was found to increase to the levels of unsteadiness that exist at high hover, and the variation of unsteady loading with wind speed is changed by the interaction of the ship airwake and rotor downwash. Generally the unsteady loading increases with the additional influence of main rotor downwash compared to the baseline, rotorless case. The wind tunnel data, particularly side

force and drag, are then shown to correlate well with flight-test derived operational limits. The correlation of unsteady yawing moment with the operational limit is less straight forward.

Nomenclature

R	Rotor radius
V	Wind reference speed
μ	Advance ratio
Ω	Rotor rotational speed

Introduction

The pilots of maritime helicopters face significant challenges when operating from ships. The pilot must navigate the helicopter through the ship airwake, a complex flow field that arises from the forward motion of the ship and the interactions of the atmospheric boundary layer with the ship superstructure. The ship airwake contains spatial gradients in flow speed and direction arising from the presence of free shear layers, a zone of recirculation, large wakes, and vortex structures all of which contribute to the operational challenges confronting a pilot. Moreover, the flow topology alters with wind direction (Ref. 1). Consider the example of a frigate, which has a landing deck located directly behind a hangar towards the aft of the ship. For winds coming from the direction of the bow, the flow over the landing deck is analogous to that for a three-dimensional backward-facing step. The helicopter must traverse free shear layers which separate from the top and sides of the hangar. Beneath these shear layers, and close to the rear face of the hangar is a recirculation zone which will affect the fuselage depending on its hover position above the flight deck. As the wind direction increases above about 15 deg, the topology of the airwake becomes skewed and vortices begin to emerge from the flight-deck edges and aft corners of the hangar. The wake of large bluff-body components on the roof of the hangar may also increase pilot workload for some wind angles.

*Assistant Research Officer

†Senior Research Officer

Presented at the 29th European Rotorcraft Forum, Friedrichshafen, Germany, September 16-18, 2003. Copyright © 2003 by the National Research Council Canada.

The levels of turbulence within a ship airwake are known to be two to three times the magnitude of turbulence in the natural wind over the sea. In addition, the size of the fuselage and rotor are comparable to the turbulence length scales in the airwake flow field. The unsteadiness in the flow field has significant energy over the frequency bandwidth that affects the handling qualities of the helicopter, approximately 0.2 to 2 Hz (Ref. 2). The response of a helicopter to airwake turbulence will manifest itself as a time-varying displacement in addition to variations in attitude and heading. This response will present control problems to the pilot as he strives to maintain a relative position with the ship. Across this bandwidth the magnitude of the response spectrum will represent the portion of a pilot's workload that is focused on responding to airwake turbulence.

The landing of a helicopter on a ship is governed by ship-helicopter operating limits (SHOL), which are boundaries defined by several factors including excessive pilot workload due to turbulence in the ship airwake. Presently the envelope of the SHOL is developed almost exclusively by flight test at sea. While exploring and defining operational limits by flight test is an established methodology, it is also an expensive and sometimes limited means (e.g., due to the weather encountered during the trial) of qualifying a helicopter for shipborne operations. Progress has been made to develop high-fidelity piloted-simulation for the ship-helicopter dynamic interface as another means of defining a SHOL. The success of the United States Joint Ship Helicopter Integration Program (JSHIP) is a prime example (Ref. 3). Piloted-simulation, however, cannot currently supplant flight test as the primary means of SHOL development. In fact simulation methods are currently viewed as a complementary means that will help reduce the extent and expense of flight test. In addition, simulation methods can be useful for evaluation of the airwake of a ship during its design cycle, or of the effect of change to its in-service configuration. Piloted-simulation, in particular, will be useful for evaluating different landing schemes and for training pilots for the dynamic interface environment.

For the past three years the Aerodynamics Laboratory has been developing an experimentally-based simulation to assist with the development of SHOLs (Ref. 4, 5). The crux of the methodology lies with establishing a correlation of measured unsteady aerodynamic fuselage loads (side force, yawing moment, and drag force) with pilot workload assessed for cases where airwake turbulence is primarily responsible for the workload. Unsteady loading is determined from aerodynamic measurements within a sub-scale model of the dynamic interface environment in a wind tunnel. As shown in Fig. 1, unsteady aero-

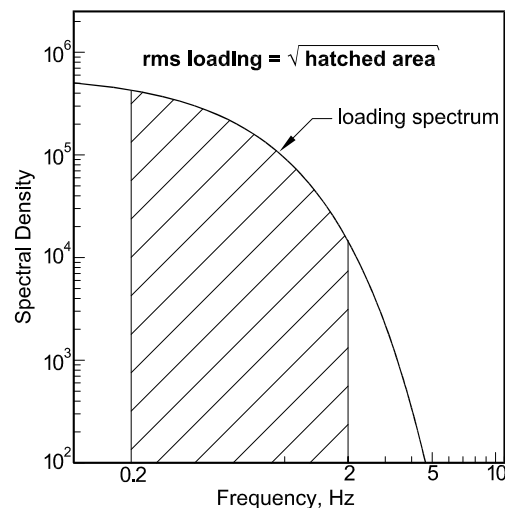


Fig. 1. Definition of root-mean-square (rms) loading.

dynamic loading is quantified by the square-root of the integral of the loading spectrum over a frequency bandwidth of 0.2 to 2 Hz. In this paper the quantity is interchangeably referred to as unsteady loading or root-mean-square (rms) loading. RMS loading indicates the degree of variation in the aerodynamic loading within the frequency bandwidth of interest: A high rms loading signifies a large degree of unsteadiness whereas a zero rms load indicates steady aerodynamic loading.

The wind-tunnel simulation was developed in a progressive manner. The first phase, completed in March 2001, focused on the development of a suitable technique to measure unsteady aerodynamic loading on a fuselage without a rotor in the ship airwake environment (Ref. 4). The technique was applied to a CH-124 Sea King rotorless fuselage in the airwake of a Halifax Class Canadian Patrol Frigate (CPF). A correlation between unsteady loading and pilot workload from flight trials was established from these measurements. In addition, normalized power-spectral densities were found to collapse well, allowing non-dimensional spectral curve fits to be generated (Ref. 5).

The assessment of pilot workload is represented by a qualitative score awarded during flight test. In this paper, assessments are based on the Pilot Rating Scale (PRS) which unfortunately does not specify the reason for a rating (e.g., turbulence, pedal margin, torque margin). However, the flight test points with which this paper is concerned fall within a sector of wind direction in which excessive pilot activity due to airwake turbulence was reported (Ref. 6). Thus it is reasonable to assume that the ratings are largely attributable to turbulence. Future workload assessments are expected to be made with the Deck Interface Pilot Effort Scale (DIPES). Specifically de-

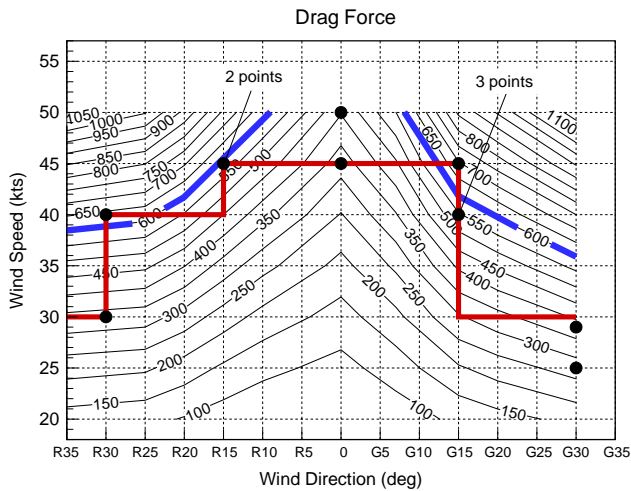


Fig. 2. Contours of rms drag force (Newtons, full scale) exerted on the fuselage of a Sea King helicopter (without main rotor) at high hover over a CPF flight deck. Black dots represent flight test points with a PRS-4 rating. The blue line denotes the rms loading corresponding to PRS 4; the red line is the existing SHOL envelope (reproduced from Fig. 9).

signed for dynamic testing at sea, DIPES ratings have greater resolution than PRS in that a suffix ascribed to the numerical rating indicates perceived cause(s) of increased pilot workload, such as airwake turbulence.

For SHOL development it is envisioned that flight test points sharing a common rating will be superimposed on contours of unsteady aerodynamic loading over a grid of wind direction and speed (Fig. 2). Note that these specific contours were developed without the main rotor in the simulation and are intended for illustrative purposes only. The contour which best fits the flight test points determines the rms loading associated with the particular rating. In Fig. 2, for example, flight test points of PRS 4 are superimposed on contours of unsteady drag force. The flight test data is taken from the qualification tests of the Sea King for the CPF (Ref. 6); the contours are based on data furnished by the aforementioned spectral fits developed for the fuselage-only experiments. The 600-N contour was judged to fit the flight test points reasonably well, and thus a rms drag force of 600 N corresponds with PRS 4. Moreover, since PRS 4 represents conditions that are judged to be the limit of a fleet pilot's capability, the magnitude of the unsteady drag force is referred to as a "rms loading limit". An rms loading limit can likewise be identified for side force and yawing moment, and also for different hover positions. In theory, the limits can be judiciously combined to form a "composite" rms loading limit. Once the composite rms loading limit is defined, an operational limit can be suggested. With this approach fewer test points are

expected to be required in the flight test program over the sector of wind directions for which airwake turbulence is the principal cause of increased pilot workload.

While the contour plot in Fig. 2 shows modest correlation with the flight-test derived operational limit, the trends were encouraging enough to undertake a second series of experiments wherein a limited-fidelity rotor was included. As will be shown, the correlation between wind-tunnel derived unsteady loads and flight-test data improved considerably. These results make it possible to consider using wind tunnel experiments to augment SHOL development.

This paper focuses on the second series of experiments, which incorporates the main rotor in the simulation. This step improves the fidelity of the simulation by including the effect of rotor downwash and the inherent coupling of rotor downwash and airwake. In the presence of rotor downwash and airwake turbulence, unsteady aerodynamic loads were measured again and the effect of the rotor on the unsteady loading of the fuselage was examined. This coupling effect has been partially incorporated in computational approaches (Ref. 7, 8) but the results are not known to have been validated.

Experimental Details

Scaling Parameters

The scaling parameters applicable to this investigation are reduced frequency, Reynolds number, and rotor thrust coefficient. Frequency scaling is necessary to correctly capture the unsteady aerodynamic loading over the full-scale bandwidth of 0.2 to 2 Hz. The test must adhere to the frequency scale because the spectra of the unsteady loads arise from the turbulent ship airwake and the rotor downwash. Reduced frequency matching relates frequency, geometric, and velocity scales. The geometric scale (i.e., the ratio of model to full scale) was fixed at 1:50 by the scale of the existing CPF model. A velocity scale of 1.1:1 was governed by the highest velocity attainable in the test section. Thus reduced frequency matching produces a frequency scale of 55:1. This scaling also ensures that the rotor advance ratio is correctly modelled.

Two Reynolds numbers are applicable to this test: fuselage and ship-based. The highest fuselage Reynolds number was approximately 1.0×10^6 based on overall length. One must be cautious, however, in defining a specific Reynolds number in the case of a fuselage immersed in a ship airwake. There are significant velocity gradients and even flow recirculation over the volume occupied by the fuselage. Thus the interpretation of the fuselage Reynolds number is not as straightforward as in the case of uniform



Fig. 3. The Propulsion Wind Tunnel at the Institute for Aerospace Research in Ottawa.

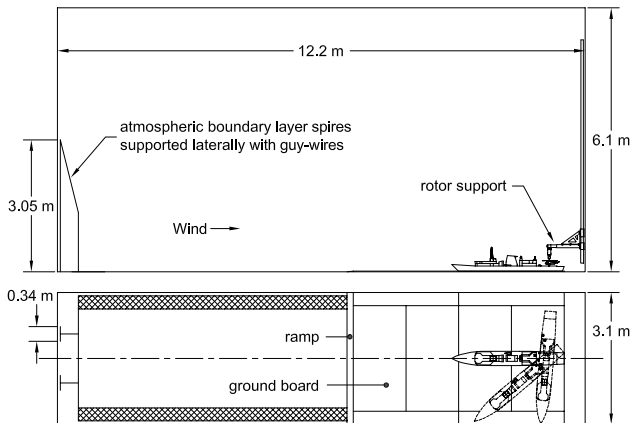


Fig. 4. Layout of test section.

flow. The Reynolds number for the ship, based on the beam, exceeds by two orders of magnitude the minimum recommended for the wind-tunnel modelling of ships (Ref. 9). Sharp-edged bodies, such as the superstructure of a ship, are not sensitive to Reynolds number, so its distortion in terms of airwake is not considered to be of concern.

The rotor thrust must be scaled to correctly represent the interaction of the airwake and rotor downwash. The issue of rotor thrust coefficient is addressed later in the discussion of the rotor model.

Wind Tunnel Facility

The experiments were conducted in the open-circuit Propulsion Wind Tunnel at the Institute for Aerospace Research in Ottawa, Canada (Fig. 3). The test section measures 3.1 m wide by 6.1 m high with an overall length of 12.2 m. The maximum sustainable wind speed is 37 m/s. A turbulent atmospheric boundary layer, consistent with a moderate sea state, was generated by a pair of boundary layer spires. A schematic of the test section appears in Fig. 4.

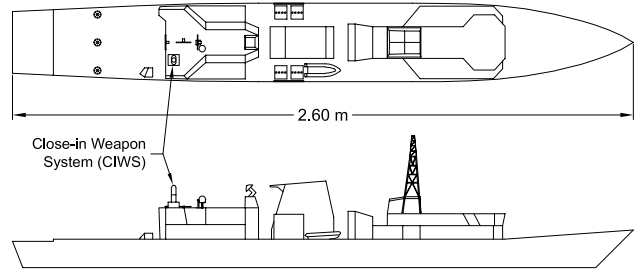


Fig. 5. 1:50-scale above-water model of the Canadian Patrol Frigate.

Description of Models

Canadian Patrol Frigate. The ship model is a 1:50-scale wooden above-water model of the CPF (Fig. 5). It features the major components such as the superstructure, radio mast, exhaust stack, and helicopter hangar. Models of smaller structures on the roof, believed to have an impact on the airwake, were also added. These include the Close-in Weapon System (CIWS), fire control radar, INMARSAT antenna dome, and the horizon/pitching bars. Small structures located in front of the helicopter hangar, such as wire antennas, handrails, a small lattice radar-mast, and 57 mm cannons were excluded from the model. From an aerodynamic perspective, the airwake should nevertheless be highly representative of a detailed CPF since the wake signatures of these small structures will blend into the flow as one moves aft. Ship motion – such as rolling, pitching, or heaving – was not considered in this test. The pitch and roll angles of the ship model were zero.

The model was placed on a ground board and could be yawed on a pivot placed near the stern of the ship. With the pivot placed on the centreline of the test section, the CPF could be rotated to simulate wind directions up to 30 deg to either side before the bow contacted the walls of the test section (Fig. 4). Wind directions greater than 30 deg were simulated by shifting the model laterally to another pivot hole in the ground board.

Fuselage Model. The 1:50-scaled model of the Sea King fuselage features representations of major com-



Fig. 6. 1:50-scale model of the CH-124 Sea King fuselage.

ponents (Fig. 6). Details such as the tail rotor, air/surface search radar, electric cable winch, sonobuoy launchers, and various antennas were considered nonessential for unsteady load measurements and omitted from the model. A model of a tail boom strake was added to the fuselage for this test.

The fuselage model was manufactured, under numerical control, from structural plastic foam so that the model would be lightweight. For this test the pitch and roll angles of the fuselage were zero. Also the longitudinal axis of the fuselage model was always aligned with that of the CPF, which is typical for a landing maneuver.

Rotor Model. As previously discussed the purpose of this test was to increase the fidelity of the wind-tunnel simulation by incorporating a scaled Sea King main rotor. At a geometric scale of 1:50, however, it was not considered possible to include a fully articulated rotor. Instead a rigid aluminum rotor with a scaled diameter of 37.8 cm was incorporated (Fig. 7). Collective angle was set by manually adjusting the pitch angle of each blade. With a prototype rotational speed of 203 rpm and a frequency scaling of 55:1, the model-scale rotor rotational speed was 11,200 rpm.

Matching rotor diameter and thrust coefficient were considered of primary importance, based on the experience of previous experiments (Ref. 10). Those results demonstrated that changes to time-averaged rotor thrust coefficient due to variable inflow (airwake) at model-scale were consistent with full-scale data. For the present test a nominal value of 80 kN was selected as representative of a typical landing weight for the Sea King. This weight corresponds to a nominal thrust coefficient of 0.00578. During the experiment the thrust coefficient was held to within 10% of the nominal target. Since the rotor thrust varies with inflow velocity, it was not considered an efficient use of wind tunnel time to trim the rotor precisely for the desired thrust coefficient. It was also recognized that

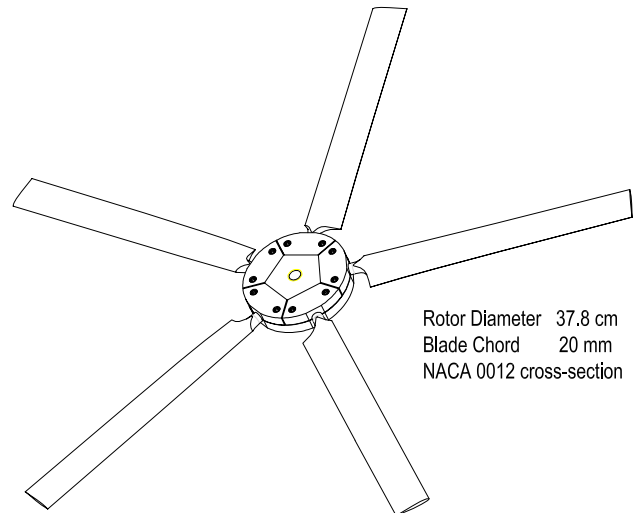


Fig. 7. 1:50-scale model of the CH-124 Sea King main rotor.

the landing weight will vary in practice with fuel levels, mission kit, and on-board personnel, so a range of thrust coefficients was considered acceptable.

Like the prototype, the model rotor has five blades. The model hub, however, is larger than the prototype, extending to approximately 20% of the rotor radius, in order to reduce the stresses in the blades. In practice little or no thrust is generated at these inboard locations for most rotors, so an oversized hub should not be a significant deficiency. As a further stress reduction measure, the blade chord was increased to 20 mm, almost double the length expected from geometric scaling.

The rotor was designed to match as closely as possible the variation of spanwise loading of a rotating blade. The prototype blade cross-section (NACA 0012) was retained in the model blade, however, the washout of the model blade deviated to account for the change in lift-curve slope of the aerofoil at model and full-scale Reynolds numbers. For instance, the nominal model Reynolds number at the 3/4 radius point is 165×10^3 whereas the full-scale value is 3.5×10^6 .

The rotor was decoupled from the fuselage model and driven from above by an electric motor through a gearbox with a 5.2:1 reduction ratio. A 75-mm long shaft extended from the output side of the gearbox to increase the clearance between the motor package and the rotor plane, thereby reducing the potential of the motor housing to influence the rotor inflow. The rotational speed of the rotor was optically detected from this shaft. The motor operated under open-loop control at about 58,000 rpm and typically required 1,100 W of input power.

The thrust developed by the rotor was sensed by a six-component balance fastened to the top of the



Fig. 8. The dynamic balance fits into a cavity in the fuselage model.

motor housing. All six output signals of the balance were sampled, however, only the thrust load was of interest. The motor package and balance were carried by a telescoping arm which was, in turn, supported by a large traversing mechanism. Precise control of the lateral and vertical position of the rotor was made possible by this mechanism. Longitudinal positioning of the rotor was done manually by adjusting the extension of the telescoping arm. Measures were taken to ensure the rotor remained steady at its position over the fuselage while it spun at 11,200 rpm in a turbulent airflow. To safely decouple the rotor and the fuselage, a clearance of 5 mm was maintained between the bottom surface of the rotor hub and the top surface of the fuselage. The clearance is greater than allowed by proper scaling, but was not expected to have a significant bearing on the unsteady aerodynamic loading of the fuselage.

Dynamic Balance. A dynamic balance is necessary to acquire the aerodynamic loading spectra of a helicopter fuselage in a ship airwake. This type of balance has high stiffness and is used in combination with a lightweight model. Fitting conveniently within an aluminum-lined cavity inside the fuselage model (Fig. 8), the internal balance measures side force, yawing moment and drag force in the body-axis coordinates of the fuselage. Yawing moment was resolved about the axis of the rotor shaft. The balance sits atop a sting that threads into a large steel block fitted beneath the flight deck of the CPF model. The steel block serves as a firm mechanical ground. Of the schemes the fuselage model can be mounted on a sting, the approached adopted is considered to have the least aerodynamic interference with the fuselage wake. The aerodynamic loads were not corrected for sting interference. Ideally the lowest natural fre-

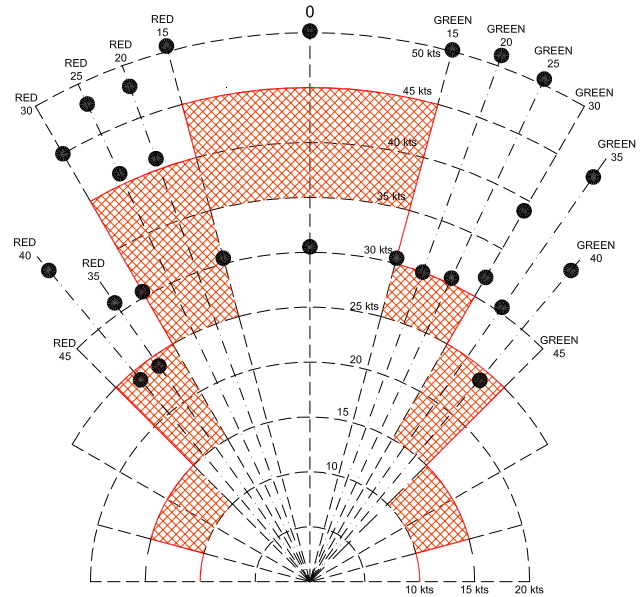


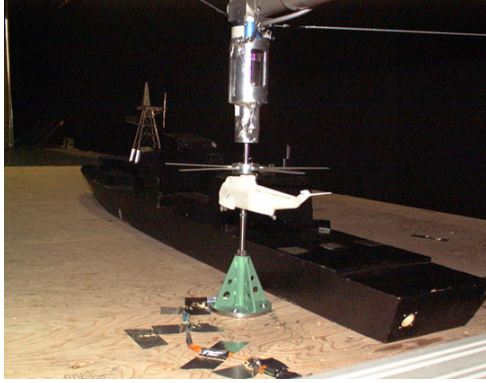
Fig. 9. Test points superimposed on the Halifax Class Freedeck Wind and Ship Motion Envelope for freedeck recoveries in daylight conditions and a moderate sea state (Ref. 6). Hatched areas indicate possibility of high workloads.

quency of the assembly is sufficiently above the frequency bandwidth of interest to prevent balance resonance from affecting measurements. If the resonant frequency is not sufficiently high, post-test spectral corrections are required.

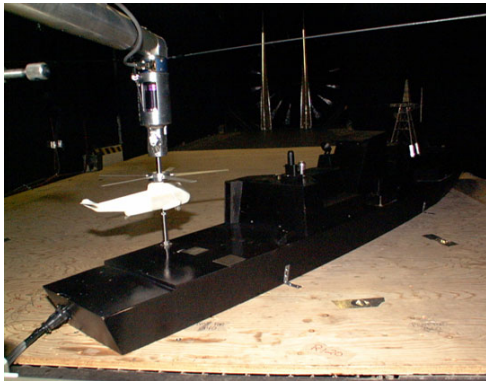
The balance was statically calibrated to a limit load of ± 20 N for side force and drag force, and ± 1 N-m for yawing moment. Functional checks of the balance demonstrated that an applied load could be recovered within about 3% of these limits. Like the rotorless tests, the resonant frequency of the model/balance/sting combination was expected to infringe on the bandwidth of interest (i.e., 11 to 110 Hz at model scale). Post-test spectral corrections to remove the effect of the mechanical transfer function, were implemented by fitting the one degree-of-freedom mechanical admittance function to a resonant peak in a least-squares fashion (Ref. 11).

Data Acquisition and Reduction. The output signals of fuselage and rotor balance were sampled at a rate of 1 kHz for a duration of 34 seconds. This corresponds to a sample rate of 18.2 Hz and a duration of 31.2 minutes at full scale. The voltage signals were converted to time-histories of force and moment in engineering units at model scale.

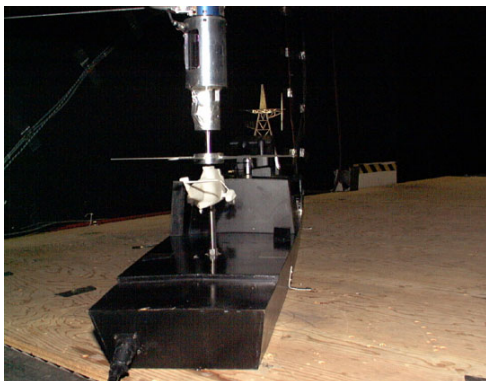
For the fuselage, power-spectral densities were computed for side force, yawing moment, and drag force from the average of sixteen 2048-point fast-Fourier transforms of the unbiased time-histories of the aerodynamic loads. Correction for the effect of



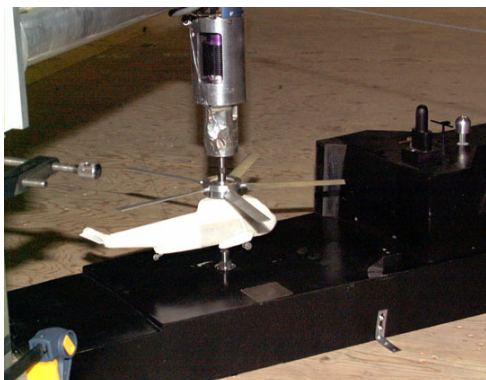
(a) High hover off-deck



(b) High hover over the port edge



(c) High hover, centred over the flight deck



(d) Low hover, centred over the flight deck

Fig. 10. Hover positions tested.

structural resonance was carried out as previously described.

Rotor thrust was computed as a simple time average.

Test Program. The test points for this investigation cover a range of wind directions between Red 45 and Green 45*. The wind directions between Green 30 and Red 30, in particular, is a sector for which excessive pilot control activity was attributed to airwake turbulence (Ref. 6). Test points were largely selected from areas of high pilot workload while some low-speed cases were chosen for the purpose of assessing the variation of unsteady loading with wind speed. Originally the wind speeds of some test points were selected to coincide with test points from flight test at sea (Ref. 6), however, wind speeds were later found to be higher than expected and the velocity scale could not be altered. All test points shown superimposed on the SHOL in Fig. 9, are plotted at the actual full-scale wind speed.

All test points were examined at four hover positions. These positions (Fig. 10) are typical of the Canadian procedure for helicopter recovery:

- High hover off the port side with rotor axis 5 m full-scale (similar to delta hover)
- High hover over port edge (similar to the hoist position)
- High hover, centred over flight deck
- Low hover, centred over flight deck

In the 'low' hover position, the rotor plane is 6 m (full scale) above the flight deck; in 'high' hover, the rotor plane is 9 m above the deck.

Results and Discussion

All unsteady loading results are expressed at full-scale magnitude in engineering units and are referenced with respect to standard air density. The reference wind speed (hereafter referred to as wind speed) is the ship anemometer speed.

Typical Loading Spectra. Typical loading spectra of side force, yawing moment, and drag force are shown in Fig. 11. Spectra with and without the presence of rotor downwash are compared for each load component. Generally the shapes of the spectra are consistent and the low-frequency end of all spectra dominates the loading. A comparison of the power spectra for each load component indicates an increase of unsteadiness under the influence of the downwash for

* 'Red' signifies a wind from the port side of the ship, and 'Green' is a wind from the starboard side.

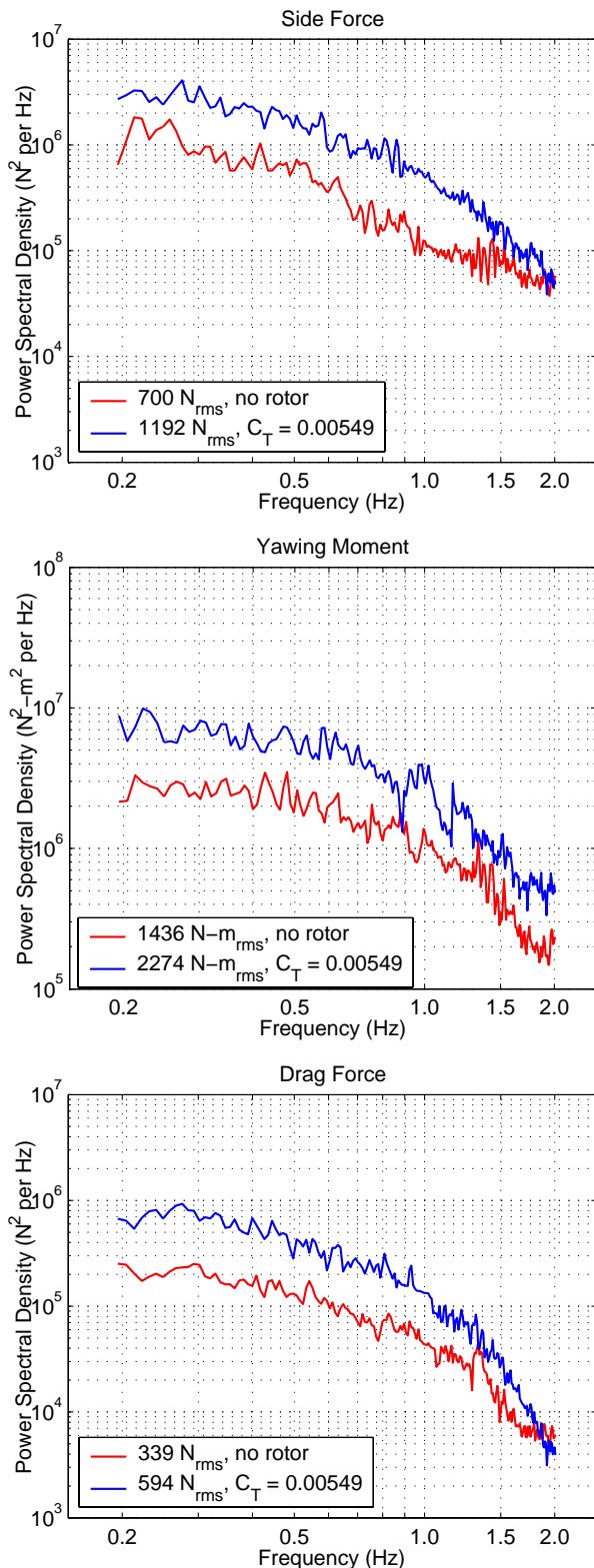


Fig. 11. Typical full-scale power-spectral densities and rms loadings for side force, yawing moment, and drag force. Wind: 0 deg, 51 kts. Position: High hover, centred over flight deck.

the indicated wind direction, speed, and hover position. The rms loadings associated with each spectrum were computed in accordance with Fig. 1 and clearly reflect the effect of rotor downwash upon the unsteady loading of the fuselage. In the next section it will be shown that under certain conditions unsteady yawing moment due to the additional influence of the rotor will be less than without the rotor.

Effect of Wind Direction. The effect of wind direction on rms loading, with and without the rotor, is illustrated in Fig. 12. Results are shown for a fuselage centred over the flight deck at high hover for a 50-kt wind speed. For an isolated fuselage, unsteady side force, yawing moment, and drag force increase with non-zero wind direction. In Ref. 4 the increases were attributed to two factors: (1) changes in the structure of the airwake that occur as wind direction increases from zero which further exposes the fuselage to the separated shear layer from the vertical surfaces of the hangar and from vortices emanating from the edge of the deck; and (2) the wake of the fuselage, an unsteady flow field itself, enlarges as the cross-sectional area of the fuselage normal to the oncoming flow increases with wind direction. Unsteady side force and yawing moment are reasonably symmetric between Red and Green winds. A turbulent wake emanating from the Close-in Weapons System (CIWS), mounted on the hangar roof (Fig. 5), and directed towards the fuselage in a Green 15 or 20 wind is likely responsible for higher rms drag force at these wind directions.

With the influence of rotor downwash, the nature of the unsteady loading alters. In general rms loadings with rotor downwash are higher as expected; however, the results for unsteady yawing moment indicate that the loading is less under the influence of the main rotor in Red winds. This behaviour also occurred at a lower wind speed for the same hover position. Results for the three other hover positions show that the asymmetric unsteady yawing moment persists. Moreover, the asymmetry continued to exist even without an airwake, i.e., with the ship removed and the helicopter model immersed in the turbulent boundary layer only. Consequently, the behaviour of unsteady yawing moment may be a reflection of a rigid-rotor effect. A rigid rotor in an oncoming flow will generate more lift on the advancing blade than on the retreating blade. It is speculated that this unbalanced lift distribution over the rotor plane leads to an asymmetric distribution of rotor downwash that, for a counter-clockwise rotation, contributes to lowering unsteady fuselage yawing moment in Red winds. A rotor incorporating blade flapping will equalize the lift distribution. Such a modification to the rotor is being considered for the next phase of the test program.

Effect of Wind Speed. The effect of wind speed on rms loading is shown in Fig. 13. Results are pre-

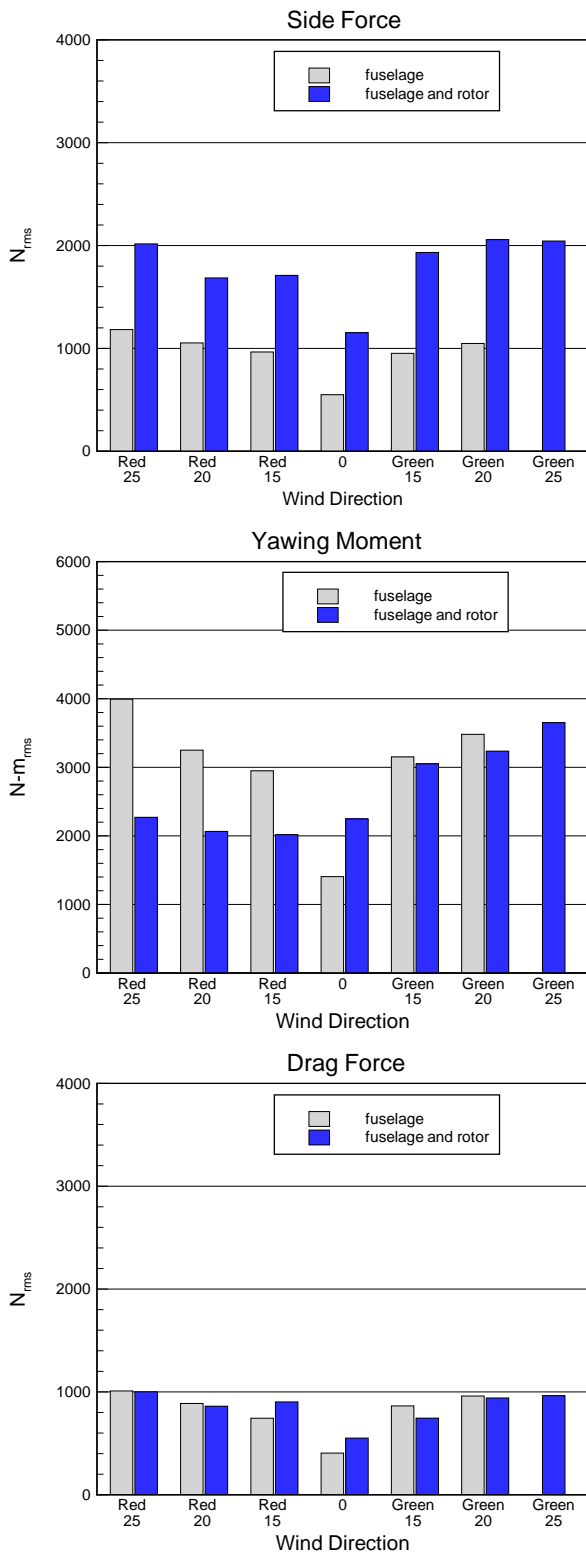


Fig. 12. The effect of wind direction on unsteady aerodynamic loading with and without the presence of the main rotor. Wind: 50 kts. Position: High hover, centred over the flight deck.

sented for each hover position in a Green-20 wind. Generally rms loading increases with wind speed for each component of unsteady loading and hover position. Clearly rms loading is not proportional to the square of the wind speed, as was shown to occur with the fuselage-only case (Ref. 4), and it is evident that the variation is affected by the interaction of the ship airwake and the wake of the main rotor. It is well understood that in forward flight the onset airflow will cause the wake of a rotor to skew, and the skew angle increases with the advance ratio μ defined as

$$\mu = \frac{V}{\Omega R}$$

where Ω is the rotational speed of the rotor. In the context of a ship airwake, V is the wind speed. Experiments with a scaled articulated rotor and a representative fuselage have shown that unsteady pressure coefficients over the rear of the fuselage can be significantly affected by the wake of the rotor as the advance ratio increases in forward flight (Ref. 12).

Effect of Hover Position. The variation of rms loadings with hover position is shown for three wind directions in Fig. 14. For 0 and Red 20, rms loading does not vary greatly with hover position. Unsteady loading over the flight deck tends to be slightly higher than over the port edge or off-deck. For Green 20, however, levels of rms loading at the off-deck position are comparable to that at other hover positions in the landing maneuver. At this position the helicopter lies in the combined wake of the hangar and exhaust stack, so higher unsteady loading under these circumstances is not surprising. In fact, high pilot workload in Green winds above 25 kts was reported during helicopter in-flight refuelling (HIFR) (Ref. 6). The occurrence of high workload was attributed to turbulence in the wake of the hangar and ship superstructure. Although the off-deck position examined in the wind tunnel was higher and closer to the port-edge of the flight deck than the standard HIFR position, the two are considered comparable.

Figure 14 also shows that unsteady loading in low hover is on a par with levels in high hover, centred over the flight deck. This is a departure from the case of an isolated fuselage for which unsteady loading tends to be lower in the low-hover position. The recirculation of the rotor downwash within the confines of the hangar face and the flight deck is likely responsible for this effect.

Correlation with Flight Test. Figure 15 replots the sector of the Sea King/CPF SHOL and the flight test points shown in Fig. 2. This sector of wind direction is that for which levels of airwake turbulence are a major contributor to pilot workload, which in turn is largely responsible for the operational limit. It is important to

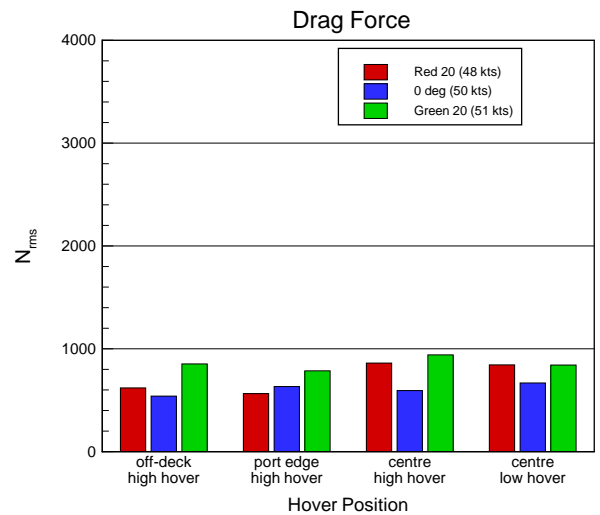
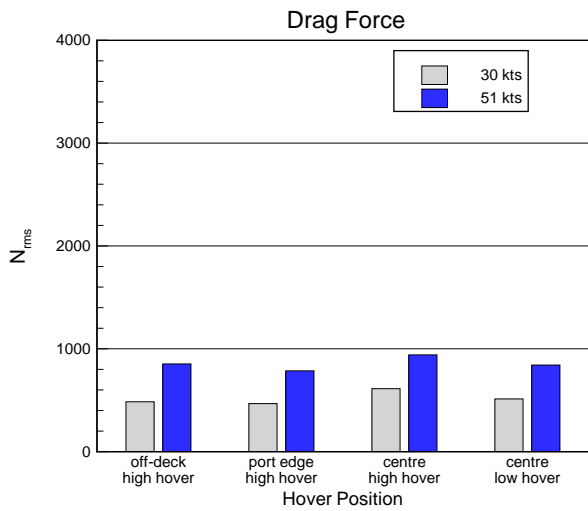
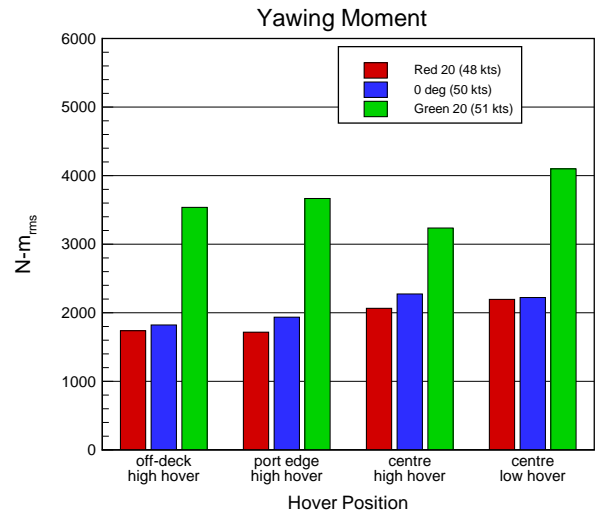
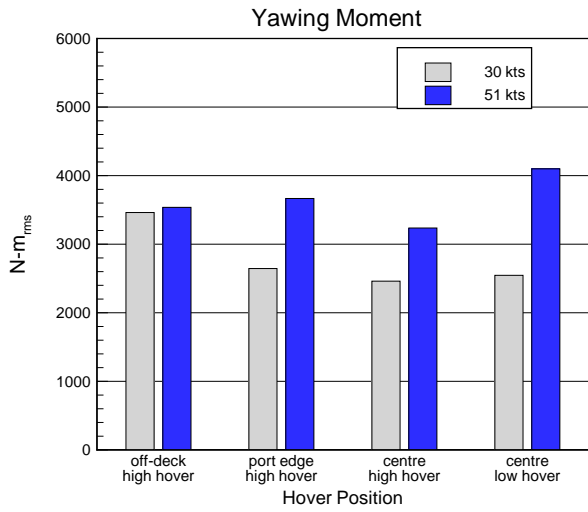
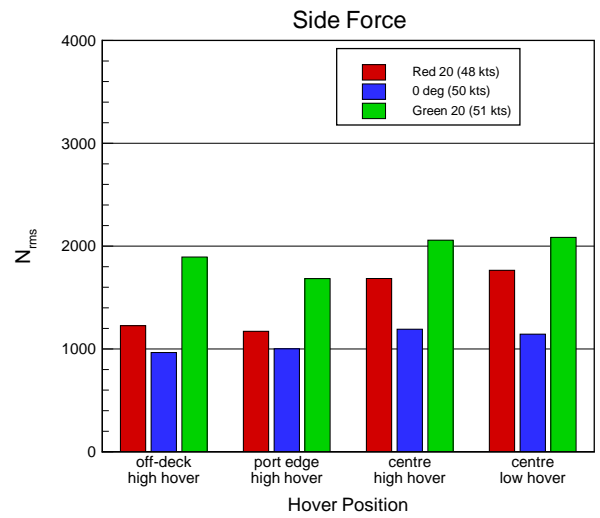
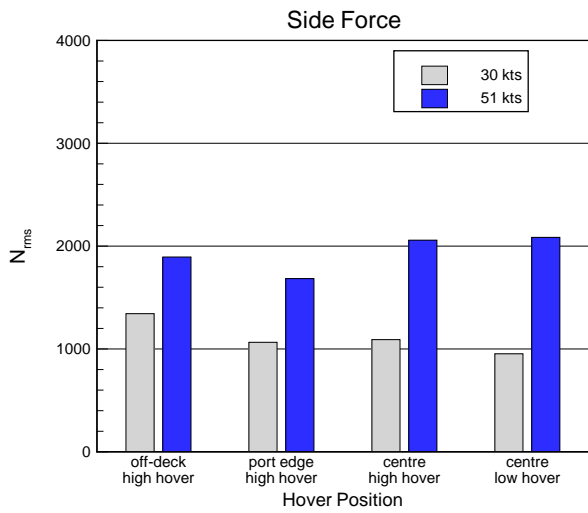


Fig. 13. The effect of wind speed on unsteady aerodynamic loading with the influence of main rotor downwash. *Wind: Green 20.*

Fig. 14. The effect of hover position on unsteady aerodynamic loading with the influence of main rotor downwash. *Wind: 50 kts.*

recall that the operational limits are restricted to following a constant wind speed (horizontal line) in 5 kt increments, or a constant direction (vertical line) in 5-deg increments. They are also derived to be conservative with respect to any flight test points that may have been acquired at wind speeds or directions falling within the increments.

Figure 15 also plots contours of constant rms fuselage loading defined from the current series of wind tunnel experiments. The measurements are taken from the rotor-spinning case with the helicopter centred over the flight deck in the high hover position. All 26 test points (Fig. 9) were used to create the contours, and it is possible that the contours could alter slightly were more data available. The drag force contour profile shows excellent agreement with the flight-test derived operational limit. The 650 N contour has been highlighted in blue and this contour appears to correlate well with the flight-test derived boundary. In particular, the drag force contours indicate sharp gradients in unsteady load at a constant wind speed as the wind direction changes from Green 15 to Green 20, consistent with the 15-kt velocity decrease in operational limit at Green 15. The contours also suggest that at 0 deg, the pilots could tolerate a wind speed of 50 kts, 5 kts above the existing limit. Thus the operational limit may not represent the physical limit for the Sea King/CPF combination.

The contours of rms side force show a reasonable correlation with the flight-envelope as well, although the gradients for winds near Green 15 are not as sharp as those for rms drag. The rms-side force contour corresponding to the operational limit appears to be about 1500 N, as indicated by the blue line in Fig. 15. Both the drag and side force contours suggest a decrease in rms load at a constant velocity as one moves from Green 25 to Green 30 winds. A decrease in airwake turbulence would be expected at about this angle, consistent with the contours. This suggests that pilots could cope with higher velocities than indicated by the flight-test derived limit. However, examination of the flight-test report reveals that the limit at Green 30 is due to the difficulty of landing a helicopter rapidly at large relative roll angles (i.e., the helicopter must be banked into the wind while the ship lists away from the wind) and is not related to airwake turbulence.

The contours of unsteady yawing moment do not follow the operational limits as closely as the drag and side force contours do. There are two interpretations of this result. One view holds that a rms yawing moment of 2700 N-m fits the operational limit well for Green winds. The fact that the operational limit does not correspond with the 2700 N-m contour for Red winds may be an indication that the combined loading in only the fore-aft and lateral axes requires suf-

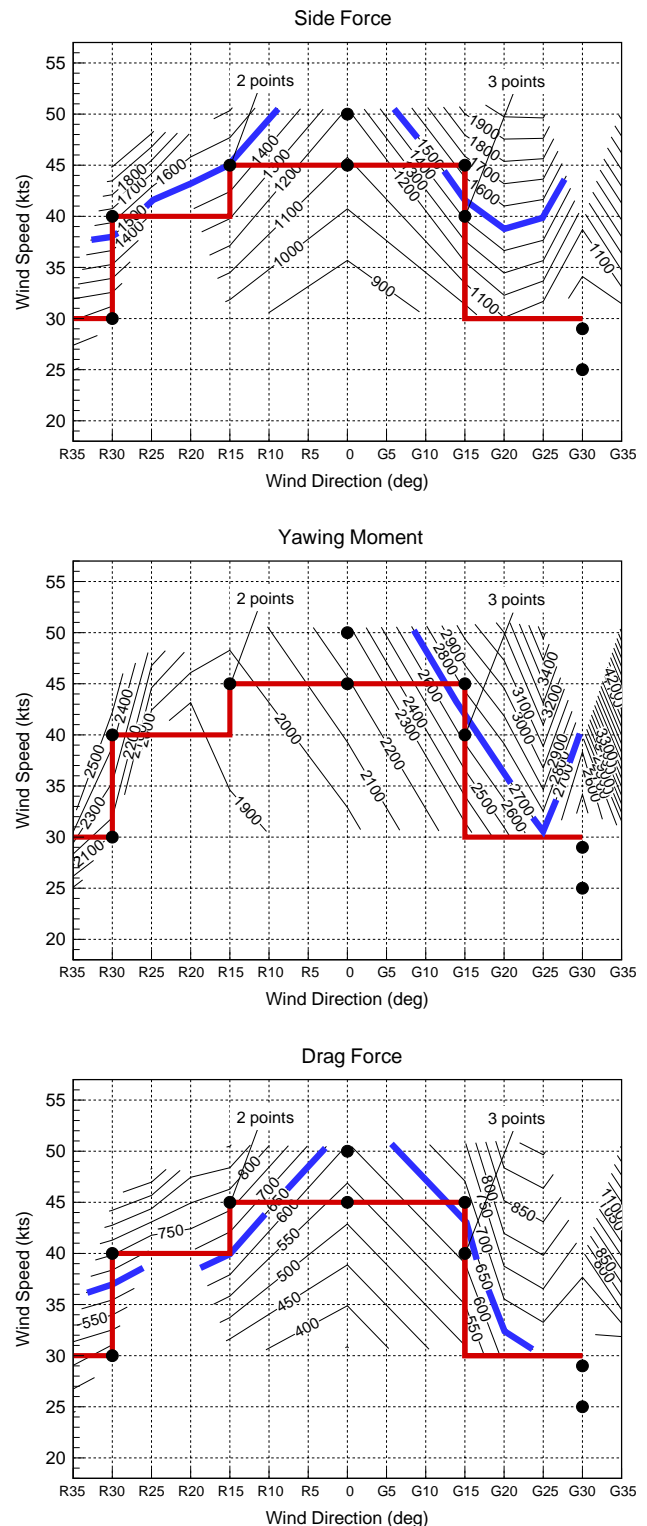


Fig. 15. Correlation of unsteady loading with flight test data. Position: high hover, centred over flight deck.

efficient pilot compensation to warrant a PRS-4 rating. This is supported by the fact that a pilot has strong lateral and vertical cues and tends to work at holding these axes first. Secondly the pilot maintains the fore-aft positioning through less frequent inputs, and lastly he controls yaw to effect changes in heading (generally only when enough capacity is available). The other interpretation of the rms yawing moment contours points to rotor fidelity, as previously discussed, and suggests that the inclusion of the flapping degree of freedom may result in changes that produce more realistic contours of unsteady yawing moment.

For the case of the fuselage and rotor in the off-deck position, the drag and side force contours for Red winds do not correlate with the operational limit (Fig. 16), since one would not expect to be limited by airwake turbulence in an off-deck position for Red winds. In general the reduced cueing environment of the off-deck position contributes significantly to pilot workload. The contour values corresponding to the operational limit are below those identified as the rms loading limit in Fig. 15, which is to be expected. Note however for Green winds that the 650 N (drag) and 1500 N (side force) limits are again close to the operational limit, since for these wind angles the helicopter is in the wake of the ship hangar.

Concluding Remarks

Experimental measurements of fluctuating side force, yawing moment, and drag force have been performed in a wind tunnel for a Sea King helicopter fuselage immersed in a ship airwake coupled with the scaled downwash of a spinning main rotor. Unsteady loading is generally higher than found previously with the rotorless case. Moreover trends of rms loading have been altered under the additional influence of the rotor downwash. In particular, the levels of unsteady loading in low hover over the flight deck were on par with that at high hover, in comparison to the rotorless case. The variation of unsteady loading with wind speed was affected by the interaction of the ship airwake and rotor downwash. These findings suggest that to conduct a proper evaluation of ship airwake effects on a helicopter fuselage in a wind tunnel, the incorporation of a correctly-scaled main rotor in the simulation is essential.

The potential to assist SHOL development with wind-tunnel measurements of unsteady aerodynamic loading is emerging. There is a strong correlation of unsteady side force and drag force with pilot workload assessed by flight test. The correlation of yawing moment with pilot workload is incomplete but shows promise. The concern expressed about the limited fidelity of the rotor model demonstrates that the development of this experimentally-based simula-

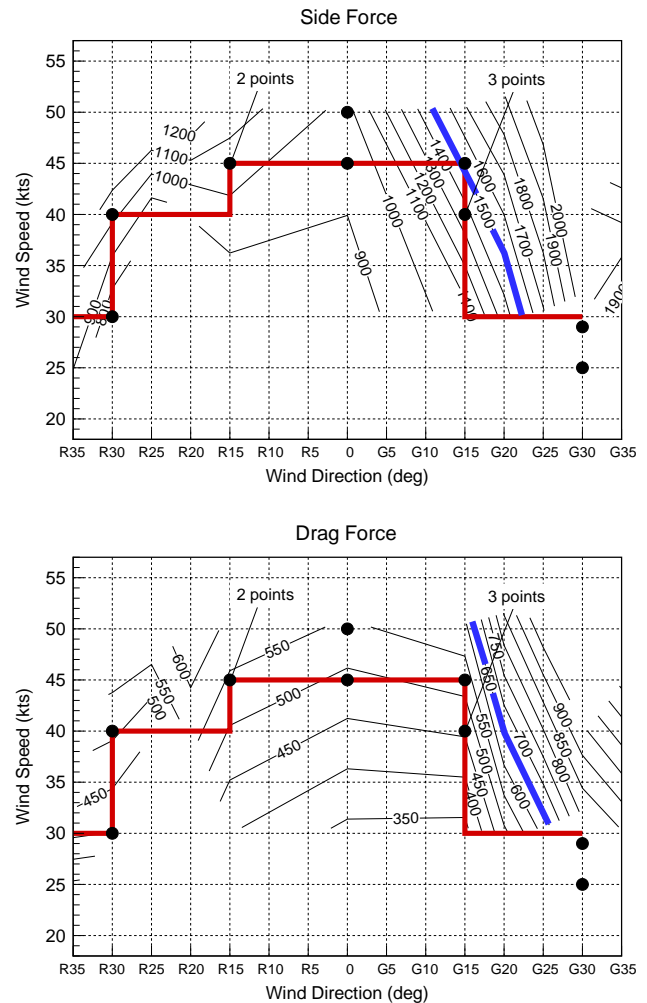


Fig. 16. Correlation of unsteady side force and drag force with flight test data. *Position: high hover, off-deck.*

tion methodology remains ongoing.

Acknowledgements

This project is a collaboration of the Department of National Defence and the Institute for Aerospace Research (IAR). The authors gratefully acknowledge the contribution of Stephan Carignan, of the IAR Flight Research Laboratory in Ottawa, on the issue of pilot workload.

References

1. Healey, J. V., "The Aerodynamics of Ship Superstructures," *AGARD-CP-509 Aircraft Ship Operations*, No. 4, 1991.
2. McRuer, D. T., "Interdisciplinary Interactions

- and Dynamic Systems Integration," *International Journal of Control*, Vol. 59, No. 1, 1994, pp. 3–12.
3. Roscoe, M. F. and Wilkinson, C. H., "DIMSS – JSHIP's Modeling and Simulation Process for Ship/Helicopter Testing & Training," AIAA Paper 2002-4597, August 2002.
 4. Lee, R. G. and Zan, S. J., "Unsteady Aerodynamic Loads on a Helicopter Fuselage in a Ship Airwake," *Proceedings of the American Helicopter Society 58th Annual Forum, Montreal, Canada*, June 11-13 2002, Accepted for publication in the *Journal of the American Helicopter Society*.
 5. Lee, R. G. and Zan, S. J., "Wind Tunnel Testing to Determine Unsteady Loads on a Helicopter Fuselage in a Ship Airwake," *Proceedings of the 23rd International Council of the Aeronautical Sciences Congress, Toronto, Ontario*, No. 2002-3.11.1, September 8-13 2002.
 6. Carignan, J. R. P. S. and Korwin-Szymanowski, M. M., "CH-124A Canadian Patrol Frigate Flight Deck Qualification," Aerospace Engineering Test Establishment Report 88/26, June 30 1994.
 7. Landsberg, A. M., Boris, J. P., Sandberg, W., and Young, T. R., "Analysis of the Nonlinear Coupling Effects of a Helicopter Downwash with an Unsteady Airwake," AIAA Paper 95-0047, January 1995.
 8. Tattersall, P., Albone, C. M., Soliman, M. M., and Allen, C. B., "Prediction of Ship Air Wakes Over Flight Decks Using CFD," *RTO-MP-15 Fluid Dynamics Problems of Vehicles Operating Near or in the Air-Sea Interface*, No. 5, February 1999.
 9. Healey, J. V., "Establishing a Database for Flight in the Wake of Structures," *Journal of Aircraft*, Vol. 29, No. 4, July-August 1992, pp. 559–564.
 10. Zan, S. J., "Experimental Determination of Rotor Thrust in a Ship Airwake," *Journal of the American Helicopter Society*, Vol. 47, No. 2, April 2002, pp. 100–108.
 11. Larose, G. L., Agdrup, K., and Larsen, S. V., "Direct Measurements of the Aerodynamic Admittance of Large Ships," *Wind Engineering into the 21st Century*, edited by Larsen, Larose, and Livesey, A. A. Balkema, Rotterdam, 1999, pp. 1939–1944.
 12. Bi, N. and Leishman, J. G., "Experimental Study of Aerodynamic Interactions between a Rotor and a Fuselage," *Proceedings of the AIAA 7th Applied Aerodynamics Conference, Seattle, WA*, No. 89-2211-CP, 31 Jul - 2 Aug 1989, pp. 428–439.